Proceedings of Meetings on Acoustics

Volume 19, 2013 http://acousticalsociety.org/


ICA 2013 Montreal
Montreal, Canada
2 - 7 June 2013

## Speech Communication
## Session 5aSCa: Flow, Structure, and Acoustic Interactions During Voice Production I

# 5aSCa1. The influence of thyroarytenoid and cricothyroid muscle activation on vocal fold stiffness and eigenfrequencies

**Zhaoyan Zhang* and Jun Yin**

***Corresponding author's address: UCLA School of Medicine, 31-24 Rehab Center, Los Angeles, CA 90095, zyzhang@ucla.edu**

The influence of the thyroarytenoid (TA) and cricothyroid (CT) muscle activation on vocal fold stiffness and eigenmodes was investigated in a muscularly-controlled continuum model of the vocal folds. Unlike the general understanding that TA contraction reduces cover stiffness, this study showed that, with reference to the resting state of zero strain, vocal fold stiffness in both layers increased with either vocal fold elongation or shortening. As a result, whether vocal fold eigenfrequencies increased or decreased with CT/TA activation depended on whether the CT/TA interaction increased or decreased the degree of existing vocal fold deformation. For conditions of strong CT activation and thus an elongated vocal fold, increasing TA contraction reduced the degree of vocal fold elongation and thus reduced vocal fold eigenfrequencies. For conditions of no CT activation and thus a resting or slightly shortened vocal fold, increasing TA contraction increased the degree of vocal fold shortening and thus increased vocal fold eigenfrequencies. In the transition region of a slightly elongated vocal fold, increasing TA contraction first decrease and then increased vocal fold eigenfrequencies. These results indicated that vocal fold eigenfrequencies were determined primarily by vocal fold stiffness rather than vocal fold stress. [Work supported by NIH].

Published by the Acoustical Society of America through the American Institute of Physics

 [DOI: 10.1121/1.4799450]
Received 22 Jan 2013; published 2 Jun 2013

# INTRODUCTION

According to the body-cover theory of phonation (Hirano, 1974), different combinations of the contraction levels of the cricothyroid (CT) and thyroaryenoid (TA) muscles can produce different stress conditions in the vocal folds and different voice types. Despite this importance, there has been no systematic and quantitative investigation of how and to what extent activation of laryngeal muscles, and especially the interaction of the CT and TA muscles, affects the stiffness of the different layers of the vocal folds, and the resulting vibration, acoustics, and voice quality. Our current understanding, based on the body-cover theory, remains largely qualitative. A more quantitative and physically-based description of laryngeal muscle activation is necessary to fully understand the role of individual and coordinated laryngeal muscle activation in vocal fold posturing and control of phonation.

Such quantitative and physically-based understanding of the muscular regulation of vocal fold geometry and stiffness is particularly important to understanding the pitch control mechanisms during phonation. Although it is generally accepted that activation of the CT muscle increases fundamental frequency (F0), the role of the TA muscle in F0 control still remains controversial. Despite many previous experimental and theoretical investigations, it still remains unclear under what conditions F0 will rise, fall, or stay constant with increasing activity of the TA muscle in humans (Titze et al., 1988). Early models of pitch control are based on the ideal string model of the vocal fold, which states that the fundamental frequency of vibration increases with vocal fold tension but decreases with vocal fold elongation. In order to relate fundament frequency to contractions of the TA/CT muscles, Titze et al. (1988) extended the string model to a body-cover two layer vocal fold model. In this modified model, although the vocal fold was still simplified as a string, the vocal fold stress now had contributions from both the body and cover layer. In addition to the passive stress, the active stress due to TA contraction was multiplied by a effective vibration depth ratio of the TA muscle and added to the passive stress. With this modified model, they showed that increasing TA activities can either increase or decrease vocal fold eigenfrequencies, depending on the depth of the body layer involved in vibration. However, the effective depth of vibration is a dynamic variable and cannot be determined a priori. It is still unknown how much control humans have over the effective depth of vibration (Titze et al., 1988). In another study, Titze and Story (2002) developed rules that relate muscle activation to the model constants of a bar-plate model, and used this model to investigate the influence of CT and TA contraction on the eigenmodes of the bar-plate model. However, the model constants of lumped-element models are difficult to be related to realistic directly measurable variables, and the rules are difficult to be translated to vocal fold models of realistic geometry and material properties.

The goal of this study was to develop a continuum finite-element model of laryngeal muscle activation, with the focus of understanding the effects of laryngeal muscle activation, particularly the interaction between the CT and TA muscles, on vocal fold geometry and stress distribution. This model was then used to investigate the influence of CT and TA contraction on the in vacuo eigenmodes of the vocal fold. Because phonation onset generally results from synchronization of the first few eigenmodes (Zhang et al., 2007), investigation of how muscle activation affects the first few eigenfrequencies would provide insights towards the muscular control mechanisms of phonation frequency.

# METHODS

A sketch of the vocal fold model is shown in Fig. 1. A body-cover two-layer simplification of the vocal folds with uniform cross-section along the anterior-posterior direction was used. The lateral surface of the vocal fold was constrained in the medial-lateral and inferior-superior directions but was able to slide in the anterior-posterior direction. As this study focused on the effects of CT/TA contraction, the posterior surface of vocal fold was fixed, simulating the condition of strong contraction of the lateral cricothyroid muscle and the interarytenoid muscle. The vocal fold was attached anteriorly to a rigid thyroid cartilage layer which was also under the influence of the CT muscle. The side surfaces of the cartilage layer were constrained in the transverse plane but was allowed to slid in the anterior-posterior direction.

## A. Constitutive equations of the vocal fold

The stress-strain relation of the vocal folds was defined using a strain energy function:

$$S_{ij} = \frac{\partial W}{\partial E_{ij}} \tag{1}$$

where $W$ is the strain energy function, $S_{ij}$ is the second Piola-Kirchhoff stress tensor, and $E_{ij}$ is the Lagrangian strain tensor. The strain energy function includes two components:

$$W = W^{passive} + W^{active} \tag{2}$$

where $W^{passive}$ and $W^{active}$ are the passive and active components of the strain energy function, respectively. The passive stress-strain relation of the vocal fold was described using a five-parameter Mooney-Rivlin model:

$$W^{passive} = c_{10}(\bar{I}_1 - 3) + c_{01}(\bar{I}_2 - 3) + c_{20}(\bar{I}_1 - 3)^2 + c_{11}(\bar{I}_1 - 3)(\bar{I}_2 - 3) + c_{02}(\bar{I}_2 - 3)^2 + \frac{1}{d}(J-1)^2 \tag{3}$$

where $\bar{I}_i$ are the modified principal invariants of Cauchy-Green deformation tensor (Holzapfel et al., 2000), and the coefficients $c$ and $d$ are model constants. Since both the vocal fold cover and muscles were assumed incompressible, $J = 1$ and thus the last term in the right hand side of Eq. (6) disappears. The model constants in Eq. (3) were estimated by curve fitting the experimentally measured stress-strain curve as reported in Zhang and Siegmund (2007), which was obtained in a tensile testing experiment using an excised human vocal fold cover. The experimentally measured stress-strain curve and the curve-fitted five-parameter Mooney-Rivlin model are shown in Fig. 2. The estimated model constants are listed in Table 1. For simplicity, the same passive stress-strain relation was used for the whole vocal fold volume including both muscles and the cover layer.

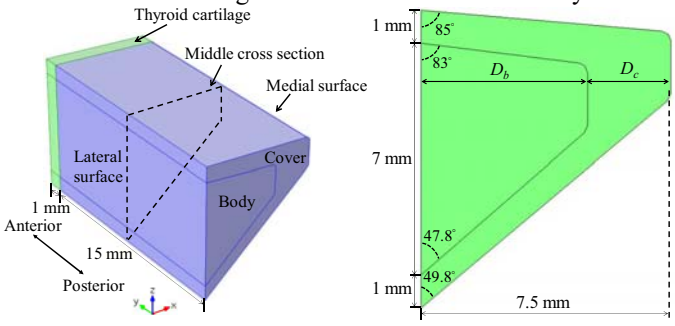


**FIGURE 1.** A sketch of (a) the vocal fold model and (b) its cross section.

**TABLE 1.** Model constants of the constitutive equation.

| **Parameter** | $c_{10}$ | $c_{01}$ | $c_{11}$ | $c_{20}$ | $c_{02}$ | $\sigma_{max}^{TA}$ | $\sigma_{max}^{CT}$ | $\lambda_{ofl}$ |
|---|---|---|---|---|---|---|---|---|
| Values | $10^4$ Pa | -8.5×$10^3$ Pa | -2.5×$10^4$ Pa | 1.8×$10^5$ Pa | -7×$10^4$ Pa | 1.05×$10^5$ Pa | 2.10×$10^5$ Pa | 1.4 |

The active component of the strain energy function was derived by considering a uniaxial motion due to the activation of an incompressible muscle fiber oriented along the AP direction, in which case the active stress along the fiber direction is related to the fiber stretch as:

$$\sigma_{active} = \lambda \frac{\partial W^{active}}{\partial \lambda} \tag{4}$$

where $\lambda$ is the muscle fiber stretch along the fiber direction. In general, the active stress depends on both the strain and strain rate, i.e. vocal fold deformation and the active stress vary with time for a constant level of muscle contraction before they reach steady-state. As this paper focuses on the steady-state vocal fold deformation and stress distribution under a given muscle activation level, the active stress was assumed to be independent of the strain rate and scale linearly with the activation ratio (level) $\alpha$ as:

$$\sigma_{active} = \alpha \sigma^{\max} f^{active}\frac{\lambda}{\lambda_{ofl}} \tag{5}$$

where $\lambda_{ofl}$ is the optimal stretch of muscle fiber at which maximum active stress occurs, $\sigma^{\max}$ is the maximum activation stress, and $f^{active}$ is the normalized function of muscle active force. In this study, the normalized function of active force $f^{active}$ as described in Blemker et al. (2005) was used:

$$f^{active} = \begin{cases} 1 - 4\left(1 - \dfrac{\lambda}{\lambda_{ofl}}\right)^2, & 0.6\lambda_{ofl} \le \lambda \le 1.4\lambda_{ofl} \\ 0, & 0.6\lambda_{ofl} > \lambda \text{ and } \lambda > 1.4\lambda_{ofl} \end{cases} \tag{6}$$

The active component of the strain energy function was obtained by substituting Eqs. (5) and (6) into Eq. (4), noting that the active stress is uniaxial along the fiber direction,

$$W^{active} = \begin{cases} \dfrac{\alpha\sigma^{\max}}{3}\left[4\left(1-\dfrac{\lambda}{\lambda_{ofl}}\right)^2 - 3\right]\left(1-\dfrac{\lambda}{\lambda_{ofl}}\right), & 0.6\lambda_{ofl} \le \lambda \le 1.4\lambda_{ofl} \\ 0, & 0.6\lambda_{ofl} > \lambda \text{ and } \lambda > 1.4\lambda_{ofl} \end{cases} \tag{7}$$

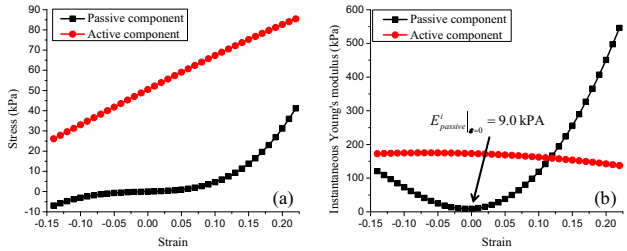


**FIGURE 2.** (a) Constitutive curve of active and passive components of vocal fold. (b) Active and passive equivalent instantaneous Young's modulus of vocal fold based on Eq. (11).

Although the CT muscle is oriented vertically in humans, contraction of the CT muscle produces a horizontal force to the vocal folds. Thus, for simplicity, the effect of CT contraction was modeled in this study as an external distributed force applied horizontally to the anterior surface of the thyroid cartilage layer. Similarly to the modeling of the TA muscle, the external force exerted on the anterior surface due to CT activation was modeled as:

$$F_A = S_A \cdot \boldsymbol{\sigma}^{CT}_{active} = S_A \cdot \boldsymbol{\alpha}_{CT}\boldsymbol{\sigma}^{CT}_{max} f_{active}\frac{\boldsymbol{\lambda}_{CT}}{\boldsymbol{\lambda}_{ofl}} \tag{8}$$

where $S_A$ is the area of cross section of CT muscle and $\sigma^{CT}_{\max}$ is the CT maximum activation stress. The stretch of the CT muscle $\lambda_{CT}$ was calculated as:

$$\boldsymbol{\lambda}_{CT} = \frac{L_{CT} - v_{Th}}{L_{CT}} \tag{9}$$

where $L_{CT}$ = 15 mm is the original length of CT muscle, which is set as the same length as TA muscle, and $v_{Th}$ is the average AP displacement of the thyroid cartilage layer. For simplicity, all other material parameters of CT, including the muscle activation function $f_{active}$, were set the same as the TA, except for the maximum active stress ($\sigma_{active}$).

## B. Pre-stressed eigenvalue analysis

Unlike the eigenvalue analysis of linear materials, for hyperelastic materials effects of initial stress and strain within the vocal folds need to be considered in the eigenvalue analysis. Thus, in this study, the analysis procedure included two steps. In the first step a static analysis was performed to calculate the static deformation and stress distribution within the vocal folds under a given conditions of CT/TA activation. Then, the eigenvalue analysis is performed on the deformed configuration of vocal fold taking into consideration of the initial stress and strain as obtained from step I.

The governing equation for the pre-stressed eigenvalue analysis is

$$[M]\ddot{\vec{q}} + ([K_c] + [K_s])\vec{q} = 0 \tag{10}$$

where [$M$] is the mass matrix, and $\vec{q}$ is the vector of generalized coordinate. The stiffness matrix consisted two contributions. The [$K_c$] matrix is the constitutive stiffness matrix, which is determined by the constitutive model, and [$K_s$] is the initial stress matrix generated due to the initial stress in the vocal fold before the eigenvalue analysis.

For nonlinear materials such as the hyperelastic material model used in this study, the [$K_c$] matrix is a function of the vocal fold strain, and thus has different values at different conditions of CT/TA activation. This contrast with linear materials for which the Young's modulus remains constant during deformations. For convenience of discussion, we define an equivalent instantaneous Young's modulus as:

$$E^i = \frac{\partial \boldsymbol{\sigma}}{\partial \boldsymbol{\lambda}} = \frac{\partial}{\partial \boldsymbol{\lambda}}\left(\boldsymbol{\lambda}\frac{\partial W}{\partial \boldsymbol{\lambda}}\right) \tag{11}$$

The instantaneous Young's modulus consisted both a passive and an active component. The dependence of the passive and active instantaneous Young's moduli on corresponding vocal fold strain is shown in Fig. 2b. Note that the minimum Young's modulus occurred at condition of zero strain and increases with change in stress in any directions (either tensile or compressive).

# RESULTS

## A. Vocal fold deformation

Figs. 3a-b shows the contour plots of vocal fold elongation and maximum medial bulging as a function of the contraction levels of the CT and TA muscles. The maximum medial bulging was calculated as the maximum medial-lateral displacement along the medial surface in the middle cross section of the vocal fold. Fig. 3 shows that changes in vocal fold length depended on the relative strength of the CT and TA muscles. Contraction of the CT muscle elongated the vocal fold, whereas TA activity shortened the vocal fold. In this study, the CT muscle had the same cross-sectional geometry as the TA muscle but was twice as stronger in the maximum activation stress. Therefore, the contour lines for vocal fold elongation were roughly anti-symmetric along the straight line $\alpha_{CT} = 2\alpha_{TA}$ in Fig. 3(a), with maximum elongation occurring at $\alpha_{CT} = 1$ and $\alpha_{TA} = 0$ and maximum shortening occurring at $\alpha_{CT} = 0$ and $\alpha_{TA} = 1$.

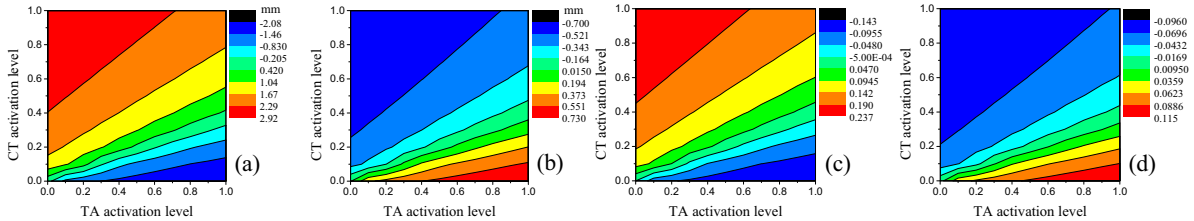


**FIGURE 3.** Contours of (a) vocal fold elongation, (b) maximum medial bulging in the middle cross section, (c) average AP strain $\varepsilon_y$ on the middle cross section, and (d) average transverse strain $\varepsilon_x$ on the middle cross section.

Due to incompressibility, changes in vocal fold length were accompanied by changes in the transverse cross-sectional geometry. Specifically, as the vocal fold was elongated due to strong CT contraction, the vocal fold depth along the medial-lateral direction was reduced by as much as 0.7 mm, slightly abducting the vocal folds. Similarly, vocal fold shortening due to strong TA activities caused a maximum medial bulging of 0.7 mm (Fig. 3b).

Figure 3 also shows the average vocal fold strain along the AP direction and within the transverse plane. As there was no considerable difference between the body and cover layers, the shown vocal fold strain was obtained by averaging over the entire vocal fold middle cross-section. In general, the absolute value of the AP strain was larger than that of the transverse strain.

## B. Vocal fold stress distribution

The contour lines for the AP stress distribution within the body and cover layers are shown in Fig. 4. As there was only passive stress in the cover layer, the AP stress in the cover layer was primarily determined by changes in vocal fold length. Consequently, the contour lines for the AP stress in the cover (Fig. 4a) were similar to those for the vocal fold elongation (Fig. 3a). Contraction of the CT muscle increased the AP stress in the cover layer, whereas TA contraction decreased it.

For the body layer (Fig. 4b), the AP stress had contributions from both the passive stress and the active stress from TA contraction. For the strain range observed in this study (0-0.15), the active stress was so large that the total AP stress in the body layer was primarily determined by the active stress except for conditions around the upper left corner in Fig. 4b. Eq. (5) shows that the active stress was determined by the normalized active force function *f*, which again depended on the AP strain, and the activation level of the TA muscle. Although TA contraction shortened the vocal folds and reduced the AP strain and the normalized active force function *f*, this decrease was generally small and dominated by the increase in the activation level, especially under conditions of large positive strain at which the rate of active stress increase with strain is small. As for the CT muscle, its contraction elongated the vocal folds and increased the AP strain and thus the AP stress in the body layer. Therefore, unlike that for the

cover layer, increased activity in the TA and CT muscles both increased the averaged AP stress in the body layer (Fig. 4b).

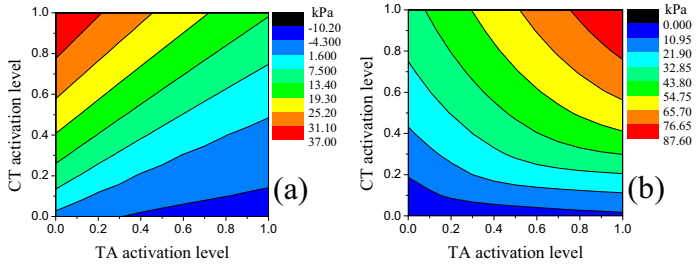


**FIGURE 4.** Contours of the average AP stress $\sigma_y$ on the middle cross section in (a) the cover layer and (b) the body layer.

Although not shown in this study, the transverse stresses were at least an order of magnitude smaller than the AP stress, with a maximum averaged stress of about 600 Pa along the medial-lateral direction and 2500 Pa along the inferior-superior direction. The shear stress in the transverse plane was about 10 Pa in the cover layer and about 600 in the body layer.

## C. Instantaneous Young's moduli

Fig. 5 shows the contour levels for the instantaneous Young's moduli within the transverse plane and along the AP direction, for both the body and cover layers, as calculated accordingly to Eq. 11.

As the transverse instantaneous Young's moduli in both layers and the AP instantaneous Young's modulus in the cover layer contained no contributions from TA activation, the contour plots for these instantaneous Young's moduli are similar to that of vocal fold elongation or stain. However, a distinction between the Young's moduli and the vocal fold strain is that the minimum values of the instantaneous Young's moduli were obtained at conditions of zero strain rather than largest negative strain, as discussed above in Fig. 2b. As a result, although the instantaneous Young's moduli generally increased with increasing CT activity and decreasing TA activity, this trend was reversed in the lower right corner of Fig. 5, or conditions of weak or no CT activation. In this region, the instantaneous Young's moduli increased with increasing TA activity and decreasing CT activity. The contour plot for the AP instantaneous Young's modulus in the body layer (Fig. 5d) followed a generally similar pattern to other instantaneous Young's moduli, except that the region of transition exhibited a slightly complex pattern, due to extra contributions from TA activation.

In general, increasing vocal fold elongation led to increased difference between the AP and transverse instantaneous Young's modulus but there was not much body-cover stiffness differential in either the transverse plane or along the AP direction. In contrast, vocal fold shortening, especially under strong TA contractions, led to primarily a large difference in body-cover stiffness along the AP direction, but with small AP-transverse difference in cover stiffness.

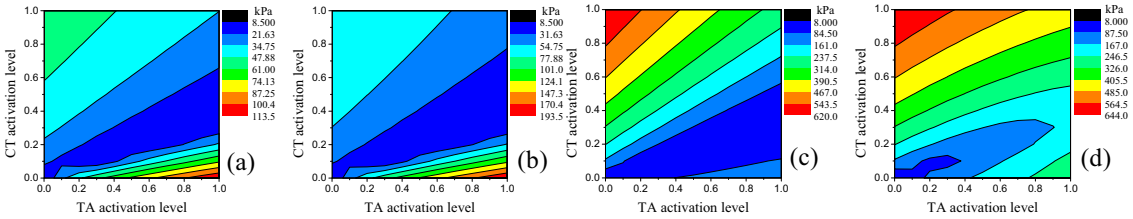


**FIGURE 5.** Contours of the instantaneous transverse Young's modulus of the (a) cover layer and (b) body layer, and instantaneous AP Young's modulus of the (c) cover layer and (d) body layer in the middle cross section.

## D. Vocal fold eigenmodes

Fig. 6 shows the contour plots of the first two eigenfrequencies. All two eigenfrequencies exhibited a similar variation pattern. Due to the imposed larger maximum activation stress of the CT, both minimum and maximum values of the eigenfrequencies were determined by the CT muscle along, with the eigenfrequencies increased by two octaves from minimum CT contraction to maximum CT contraction. CT contraction was also more effective in regulating eigenfrequencies than the TA muscle.

In the upper right portion of Fig. 6, which corresponds to conditions of vocal fold elongation, the eigenfrequencies increased with increasing CT activation and decreasing TA activation. However, the trend was reversed in the lower right portion of Fig. 6, which corresponds to conditions of vocal fold shortening. In this region, the eigenfrequencies decreased with increasing CT activation and decreasing TA activation. Non-monotonic variation patterns were also observed in the transition region. For example, the eigenfrequencies initially decreased with increasing TA(CT) activation level but then increased with further increase in TA(CT) activation level.

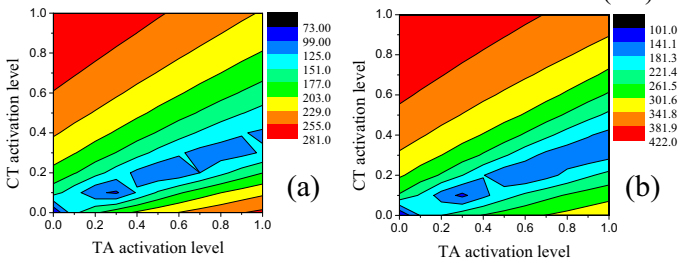


**FIGURE 6.** Contour of (a) first and (b) second eigenfrequencies.

This variation pattern of the eigenfrequencies with CT/TA contraction levels was similar to that of the instantaneous Young's moduli (Fig. 5). In contrast, although the eigenfrequency contour plots were also similar to that of the AP stress in the cover layer, they were qualitatively different in the lower right portion of the contour plots, in which the eigenfrequencies increased with decreasing AP stress in the cover. The comparisons in contour plots above thus indicated that the instantaneous Young's moduli or the constitutive stiffness played a more important role than the AP stress in determining vocal fold eigenfrequencies, at least under conditions that led to vocal fold shortening.

## DISCUSSION

Unlike the general understanding that TA contraction reduces cover stiffness, this study showed that, with reference to the resting state of zero initial stress, both elongation and shortening led to increase in vocal fold stiffness in both the body and cover layers. As a result, whether the vocal fold eigenfrequencies increased or decreased with CT/TA activation depended on whether the CT/TA interaction increased or decreased the degree of existing vocal fold deformation (Fig. 2b). For conditions of strong CT activation and thus an elongated vocal fold, increasing TA contraction reduced the degree of vocal fold elongation and thus reduced vocal fold eigenfrequencies. For conditions of no CT activation and thus a resting or slightly shortened vocal fold, increasing TA contraction increased the degree of vocal fold shortening and thus increased vocal fold eigenfrequencies. In the transition region of a slightly elongated vocal fold, increasing TA contraction first decrease and then increased vocal fold eigenfrequencies.

Similar pattern can be also observed on the influence of CT contraction on vocal fold eigenfrequencies (i.e., how eigenfrequencies change with increasing CT activity). This may seem to contradict with common experience that the CT muscle is the primary regulator of phonation frequency. However, it is noted that in this study CT contraction lowered vocal fold eigenfrequencies only at very low levels of CT contraction, which may not occur in humans in which the vocal fold is under certain AP tension even at resting state (Chhetri et al., 2011).

Previous studies estimated phonation frequency based on the ideal string model or the beam model, which considered only the AP stress. The results of this study, however, showed that vocal fold eigenfrequencies were primarily determined by vocal fold stiffness, rather than vocal fold stress. Predictions based on the ideal string model overestimated the first eigenfrequency by about 80 Hz and predicted a zero eigenfrequency at the resting state of the vocal fold. Although stiffness is closely related to stress for nonlinear materials such as the vocal folds as increase in stress also leads to increase in stiffness, they have different physical meanings: one is a property of the material itself whereas the other describes the mechanical state of the material. Previous experimental studies using vocal fold models made from linear materials have shown that phonation frequency remained almost constant during elongation (Shaw et al., 2012) and with increasing subglottal pressure (Zhang et al., 2006), confirming the relevance of vocal fold stiffness rather than stress distribution in regulation of eigenfrequencies and phonation frequency.

## ACKNOWLEDGMENTS

This study was supported by Grant No. R01 DC011299 from the National Institute on Deafness and Other Communication Disorders, the National Institutes of Health.

## REFERENCES

Blemker, S. S., Pinsky, P. M., Delp, S. L., 2005. A 3D model of muscle reveals the causes of nonuniform strains in the biceps brachii. Journal of Biomechanics 38, 657-665.

Chhetri, D. K., Zhang, Z., and Neubauer, J. (2011). “Measurement of Young’s modulus of vocal fold by indentation,” J. Voice 25, 1–7.

Hirano, M., 1974. Morphological structure of the vocal fold and it’s variations. Folia Phoniatr. 26, 89-94.

Holzapfel, G. A., Gasser, T. C., Ogden, R. W., 2000. A new constitutive framework for arterial wall mechanics and a comparative study of material models. Journal of Elasticity 61, 1-48.

Shaw, S. M., Thomson, S. L., Dromey, C., and Smith, S. (2012). "Frequency response of synthetic vocal fold models with linear and nonlinear material properties," Journal of Speech, Language, and Hearing Research **55**, 1395-1406.

Titze, I. R., Jiang, J., Drucker, D. G., 1988. Preliminaries to the body-cover theory of pitch control. Journal of Voice 1, 314-319.

Titze, I. R., Story, B. H., 2002. Rules for controlling low-dimensional vocal fold models with muscle activation. Journal of the Acoustical Society of America 112, 1064-1076.

Zhang, K., Siegmund, T., Chan, R. W., 2007. A two-layer composite model of the vocal fold lamina propria for fundamental frequency regulation. Journal of the Acoustical Society of America 122, 1090-1101.

Zhang, Z., Neubauer, J., and Berry, D. A. (2006). “The influence of subglottal acoustics on laboratory models of phonation,” J. Acoust. Soc. Am. 120, 1558–1569.

Zhang, Z., Neubauer, J., and Berry, D. A. (2007). “Physical mechanisms of phonation onset: A linear stability analysis of an aeroelastic continuum model of phonation,” J. Acoust. Soc. Am. 122, 2279–2295.